ESTIMATION OF SNOW FRACTION USING AVIRIS SIMULATED ASTER IMAGE DATA

Jiancheng Shi

Institute For Computational Earth System Science (ICESS)
University of California, Santa Barbara, CA 93106, U.S.A
Tel:805-893-2309, Fax:805-893-2578, E-mail:shi@icess.ucsb.edu

INTRODUCTION

Seasonally snow covered areas of the mountain ranges are important components in the global hydrologic cycle. Therefore monitoring the extent of the seasonal snow cover and the accumulation and ablation zones of glaciers is essential for understanding of the global hydrologic cycle, one of the objectives in the study of the Earth sciences. Seasonal snow cover is the major source of the fresh water supply over wide areas of the mid-latitudes. They account for a significant fraction of the fresh water supply. In the western U.S., for example, about 80 per cent of the total runoff comes from melting snow. Measurement of the amount of water stored in the snowpack and forecasting the rate of melt are thus essential for managing the water supply and flood control systems.

The spatial distribution of a snow covered area is a crucial input to models of hydrology and climate in alpine and other seasonally snow covered areas [1,2]. Snow covered area (SCA) is necessary to parameterize energy balance calculations in mesoscale and general circulation models [3], to initialize and validate distributed snowmelt modeling efforts [4], and to estimate snow water equivalence from observations of snow-cover depletion [5]. Because of rough, irregular topography and wind redistribution, all these attributes vary spatially and temporally over alpine areas at both coarse and fine scales. However, these important snow parameters have not been generally used in snowmelt modeling because they are difficult and costly to measure routinely over large areas.

The Airborne Visible and Infrared Imaging Spectrometer (AVIRIS) [6] flies on a NASA ER-2 aircraft at an altitude of 20 km and has a spatial resolution about 20 m over an 11-km swath. It is unique optical sensor that delivers calibrated images of the upwelling spectral radiance in 224 contiguous spectral bands in the spectral region from 0.4–2.5 μm. Its spectral resolution is 10 nm. AVIRIS has been widely used in the realm of the Earth science remote sensing [7] including atmospheric science, atmospheric correction, oceanography, ecology, and geology.

In addition, the ER-2 carries a variety of film camera. Most of the cameras and lenses are routinely calibrated for precision photogrammetry, and numerous film types are in use. Wild Heerbrugg RC-10 mapping cameras with a 9 x 9 inch (22.9 x 22.9 cm) image format are flown on virtually every ER-2 Earth imaging mission. They provide the color infrared photo with ground coverage 15 x 15 km and a nominal resolution of 1.5 to 4 m. The high resolution spectra image data (AVIRIS) and high resolution spatial color infrared photo acquired coincidentally on the ER-2 mission provide unique data sets for snow mapping algorithm development and validation.

The objective of this study is to develop an automatic snow mapping algorithm at sub-pixel resolution for Advanced Spaceborne Thermal Emission And Reflection (ASTER). It is an EOS-A facility instrument to be launched in this year. We have collected a huge amount of AVIRIS image data, from which ASTER spectral measurements can be simulated. The high resolution color infrared photo (1-4 m) taken simultaneously as AVIRIS image data can be used to access the snow covered area as the ground truth. By evaluation of the current techniques for selecting spectral endmembers and the effects of terrain on linear unmixing process, an unsupervised snow mapping algorithm has been developed by taking advantages of each technique in selecting spectral endmembers. Through examples, we demonstrate 1) effects of terrain on linear unmixing, 2) development of the unsupervised sub-pixel snow mapping algorithm, and 3) the techniques used to access the ground truth and validation of ASTER snow mapping algorithm using simulated image data from AVIRIS.

BACKGROUND

Visible and near-infrared sensors have been used extensively to delineate areas of snow and ice cover in terms of binary classification (i.e., snow or non-snow for a pixel) through supervised [1,8-9] and unsupervised classification [2, 10-11]. While snow is extremely bright in the visible wavelengths, it is dark in the short wave infrared (SWIR) wavelengths.

While alpine regions may have large areas of open snow above the tree line, patches of windblown rock or soil and shrub vegetation are also common. The spectral contributions of different materials within the field of view of the sensor result in "mixed pixels". The problem is severe over rugged terrain, where extreme variations in snow cover, vegetation type, canopy density, and lithology occur over small horizontal distances, leading to mis-classification of snow covered areas. Due to complexities of the Earth's surface, especially in rugged terrain and forest regions, large errors can be expected when using moderate to coarse resolution imagery to map snow covered areas at a regional scale.

Spectral mixture analysis has been shown to be well suited for analysis of spectral image data [12]. A spatial mixture can either be a linear or a non-linear mixture of reflectance spectra of scene materials; the difference depends on the manner in which photons scatter and interact with the materials in the pixel. In the case of linear mixing model, the sensor response for an image pixel is expressed as linear combination of the fraction quantity of each component present in the pixel plus error. Thus the pixel spectrum holds information about both the spectral signature and the abundance of a component. In a multispectral image each pixel can be modeled as a linear combination of components identified for that image. Such image components are termed "endmembers" and they are thought to be representative of a finite set of spectrally unique ingredients in the image. In terms of remote sensing, it can be represented as

$$\min(\varepsilon) = \sqrt{\frac{1}{n}\sum_{i=1}^{n}\left(R(i) - \sum_{j=1}^{m} f(j) R_e(i, j)\right)^2} \tag{1}$$

With constrains of

$$0 \le f(j) \le 1, \qquad \sum_{j=1}^{m} f(j) = 1 \tag{2}$$

Where i and j represent spectral band and endmember component in the linear unmixing. R and R_e are surface reflectance and endmember reference spectra, and f is fraction of each component. By finding minimum error ε, the fraction quantity and the spectral signature of components are determined in terms of the best fit to the measured spectral signature at a given pixel. In this way, snow cover can be mapped at sub-pixel scale and result in a fractional classification (i.e., fraction of snow cover for a pixel).

Recently, the linear spectral unmixing techniques have been applied to snow covered area classifications using AVIRIS [13-15], TM [16], and AVHRR [17]. The major difference in these studies is the techniques in selecting spectral endmembers.

1) Nolin [13-14] used 17 spectral bands with the scene manually selected spectral endmembers were obtained from the mean values of spectral reflectance from training sites for each target. It may be possible to apply the current unmixing techniques to map snow at small areas where the spectral signatures of targets have a little variation. However, great variations of spectral signatures of each target are expected at regional scales because of changes in physical properties of targets, terrain gradient and atmospheric properties (a function of elevation).

2) An unsupervised spectral unmixing algorithm, with a convex geometry technique, was used for Thematic Mapper data estimates of snow-covered areas from the six reflective TM bands [16] and AVHRR [17]. The algorithm was based on classification trees to fragment the data set along boundaries of distinct land and cloud cover classes. The dimensionality and number of endmembers for each image fragment are determined from principal component analysis. Each fragment is unmixed, with all endmember sets on its convex hull, and the best set is selected. Endmember spectra are converted to surface reflectance using an atmospheric radiative transfer code, and the endmembers

are identified by automated search of a spectral library. The final snow cover estimate is a composite of the best mixture model per pixel, adjusted for endmember impurity.

3) Painter[15] used the multi-snow endmembers simulated by the two stream radiative transfer model and multi-nonsnow endmembers obtained from field spectral measurements as described by the multi-endmember unmixing technique [18]. The study showed that the accuracy of the estimation of snow fraction can be improved by including multiple snow spectral endmembers to account for the effect of snow grain size difference.

Each technique in selection of spectral endmembers has its own advantages and disadvantages, as will be discussed in next section.

EFFECTS OF TERRAIN ON LINEAR UNMIXING

In contrast to images obtained from a flat surface, the images obtained in alpine regions show a more complicated geometric mapping. In many cases, the image data we obtained is the surface apparent reflectance after the correction of atmospheric effects, such as AVIRIS, MODIS and ASTER. The derived surface apparent reflectance is usually a function of local solar illumination angle, surface orientation, and sensor viewing geometry that affects imaged pixel size, in addition to factors that affect the surface spectral reflectance. In alpine regions, the great variations in elevation and surface orientation from pixel to pixel consistently result in a great variations in the derived surface apparent reflectance. This variation, caused by the topographic effects that are unrelated to the spectral reflection properties of surface cover type, has a great impact on classification accuracy and on the spectral linear unmixing.

Let's consider a terrain correction factor, T_c, that is needed to correct the surface apparent reflectance to real reflectance on a surface slope at a given imaged pixel. The surface apparent reflectance $R'(i,\theta)$ with

$$R'(i,\theta) = T_c R_e(i,\theta) \tag{3}$$

illumination θ is

If the spectral endmembers have no terrain effects and have the same illumination, such as those obtained from a model or field spectral measurements, the estimated fractions have properties of

As we can see, the constrains in (2) have been broken. The estimated $f'(j)$ for the dominant component could be

$$f'(j) = T_c f(j), \qquad \sum_{j=1}^{m} f'(j) = T_c \tag{4}$$

greater than 1 and sum of the estimated fractions may not equal to 1. This sum is equal to terrain calibration factor T_c, instead. This indicated that if we put (2) as constrains when applying linear unmixing, we actually excluded the real spectral endmembers. Instead, we selected a wrong combination to explain the measured spectral signals.

A commonly used technique to reduce such an effect is to normalize the estimated fractions with their

$$f(j) = f'(j) \Big/ \sum_{j=1}^{m} f'(j) \tag{5}$$

sum:

Since T_c is a constant, it will be canceled out by normalization.

However, in the case that the spectral endmembers are selected from a scene, such as using either manually selected average spectral endmembers for each component or the convex geometry technique, the reference spectral endmember for a given component j used in unmixing process has the terrain effect:

$$R'_e(j,\theta) = T_c(j) R_e(\theta) \tag{6}$$

Then, the estimated fractionts are

$$f'(j) = T_c(j) f(j) / T_c(m), \qquad \sum_{j=1}^{m} f'(j) \neq 1 \tag{7}$$

They also break the constraints of (2).

We can see that if the selected reference spectral endmembers for each component have a similar magnitude with the pixel to be evaluated, a small error can be expected. Otherwise, the opposite is true - a large error will be expected. The manually selected average spectral endmembers have fewer terrain effects on the spectral unmixing since they are generally selected over a relative flat surface and averaged over many pixels from several training sites. However, this technique does not account for spectral variability in each component. On the other hand, the technique using convex geometry has great terrain effect on spectral unmixing. This is because the spectral endmember for each component is selected at the corner of convex hull. It represents the extreme case for the spectral signature of that component and may have a large terrain effect. In addition, the normalization process of (5) also failed since the terrain effects in each component are different and can not be canceled out in the normalization.

Furthermore, it also has a great impact on spectral unmixing if the reference endmembers were obtained at a different solar illumination angle from the pixel to be evaluated. To demonstrate this effect, Figure 1 shows the two-stream radiative transfer model [19-20] simulated ratio of two illuminations at 60°/20° for three different snow conditions. The solid, dotted and dashed curves represent that for fine-grain/thick, medium-grain/thick, and medium-grain/thin snow conditions, respectively. The x-axis is wavelength in μm.

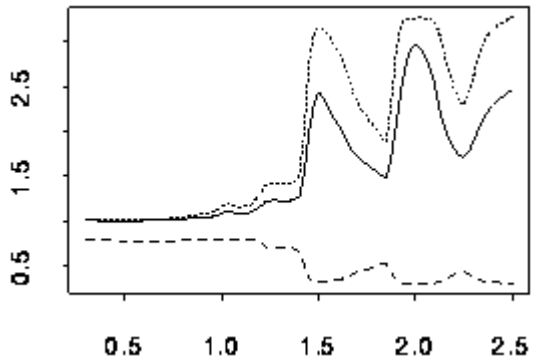

Figure 1. The ratio of reflectance at 60° to 20° illumination simulated for three snow conditions.

We can see that if the reference spectral endmembers were obtained at different solar illumination angles from the pixels to be evaluated, we will need an illumination angle correction factor to justify the difference. It is clear that this illumination angle correction factor will depend upon the different target, the difference in illumination, and the wavelength. As a result, the sum of the estimated fractions will not equal 1. The normalization process will also fail to estimate real fractions correctly.

PROPOSED TECHNIQUES

The analyses of terrain effects on spectral unmixing in the last section indicate that each technique used to select the reference spectral endmembers has its own advantages and disadvantages, when it applied spectral unmixing in mountainous areas.

1. Scene-selected spectral endmembers by either manually averaging from training sites or using convex geometry technique
    - Advantages: less sensitive to system noise, error in atmospheric correction, local spectral endmembers
    - Disadvantages: terrain and illumination effect in the selected endmembers
2. Spectral library by either field measurements or model simulation
    - Advantages: the normalization can be used to reduce terrain effect

- Disadvantages: limited available data, affected by system noise, illumination, and difference between model predications and measurements

By taking advantage of each approach, we developed a technique for automatic selection of local reference spectral endmembers. This technique mainly includes four steps:

Step 1: Level-0 classification: First perform an initial selection of possible snow, snow-free, and snow mixed pixels. It is acknowledge-based regression tree classifier. Then, we further classify these initially identified snow mixed pixels by a spectral-shape-matching classification, using the snow and snow-free spectral endmembers.

Step 2: Merge the initial selected snow, snow-free endmembers and establishing a look up table for snow mixed pixels. The similar spectral signatures in each class - snow, snow-free, and snow mixed pixels are grouped together using the criteria 1) the difference at each wave length is less than 0.02 and 2) the overall RMSE from all wave lengths is less than 0.015. Then, we averaged over those spectral signatures in each group to determine one spectral endmember signature in that class. The average process can also reduce the extreme cases in terrain effect.

Step 3: Identify local pure vegetation and bare surface spectral endmember signatures by performing multi-endmember unmixing on the selected snow-free endmembers using the spectral library obtained from field measurements. This spectral library contains more than 300 field spectral measurements, including different types of rock, soil, trees, and short vegetation. In this process, if RMSE is less than 0.015 for a snow-free endmember from multi-endmember unmixing, the spectral signatures from the library of each component will be selected and grouped into the pure vegetation and bare surface endmembers. If RMES is greater than 0.015 when it does not fit well by the measurements from spectral library, we identify the new local endmember spectral signature at a given

$$R_e(i, bare) = \left(R(i) - f'(vegetation)R_e(i, vegetation)\right) / f'(bare) \quad (8)$$

wave length *i* by

if the estimated fraction of that component is greater than 50%. In above equations, the newly determined endmember signature has a reduced terrain effect since the measurement *R(i)* and the estimated fraction f ' all have

$$R_e(i, vegetation) = \left(R(i) - f'(bare)R_e(i, bare)\right) / f'(vegetation) \quad (9)$$

same terrain effect in it and ratio process will cancel it out.

Step 4: Perform multi-endmember unmixing on the snow mixed pixel look-up table and then assign snow fractions to all pixels in that group. The advantage of using look-up tables for snow mixed pixels is that they can significantly reduce the computing time. In fact, they can generally reduce CPU time by a few hundred times at cost of only slightly reducing accuracy.

ASSESSMENT OF SNOW COVER GROUND "TRUTH"

In an attempt to develop and verify a snow-mapping algorithm, the most common problem is the lack of sufficient ground truth data. Most of snow mapping algorithms were developed and validated with only a limited or "user-supplied" set of ground truth data that covers only very small portion of snow covered environmental conditions. This type of technique cannot provide any information on evaluation of the algorithm performance and assessment in the accuracy of classification results where the ground truth was not available. It is clear that the key to validation of remote sensing snow extent product is to obtain a sufficient amount of the ground truth data which covers different background targets, terrain, atmosphere, solar and sensor viewing geometry.

Our approach to obtaining the ground truth for snow covered areas is to use the color infrared photo. It covers about 15 km x 15 km. This film, originally referred to as camouflage-detection film, differs from conventional color film because its emulsion layers are sensitive to green, red, and near-infrared radiation (0.5 μm to 0.9 μm). Used with a yellow filter to absorb the blue light, this film provides sharp images and penetrates haze at high altitudes. The color infrared photo can be digitized to three-band digital image with a pixel resolution from 1.5 to 4 m. Using the four band (near-infrared, green, red and near-infrared/green) digital color infrared photo, we classified snow-cover with a supervised classification technique, in which the minimum distance technique was

employed. The classes include snow, vegetation, water and bare ground. The snow is easily discriminated from the other targets because of its high reflectance, in contrast the water has low reflectance. The training sites of vegetation are easily selected because its high values in near-infrared and near-infrared/green bands. After obtaining the classification result, we co-registered the classification image with AVIRIS images to produce the fractional snow-covered area image.

It is evident that there are differences in the resolutions between the digital color infrared photo and AVIRIS image data because the formation of the image data differs significantly. AVIRIS image data is formed with the highest resolution at nadir along the flight line (a line). Its resolution decreases as the distance, between the sensor and imaged pixel, increase in cross track directions. On the other hand, The color infrared photo has the highest resolution at the nadir (a point) while the photo is taken. The resolution also decreases as the distance increases, but in all directions. If the imaged area is a flat surface, the primary cause of the differences in the image resolutions can be modeled using the information on aircraft tilt angle and flight height. However, terrain height in mountainous areas also results in resolutions that vary significantly. It is difficult to model these differences between these two data images due to the lack of high resolution and accurate Digital Elevation Model (DEM). In addition, another error source may be introduced during the process of scanning the color infrared photo. Due to the irregular change in the ratio of resolutions between them, the tradition used co-register technique – using tie points also provides inaccurate result.

In order to access large amounts of the accurate ground truth for snow covered areas, the technique we used to auto-co-register the high resolution digitized color infrared photo data to AVIRIS image data is the splint-window auto-correlation technique. We first divided the AVIRIS image data into the reference window boxes that are generally larger than 20 x 20 pixels. By varying the sizes and the image coordinates of the digitized color photo window box, the match-location and the resolution ratio between these two data at each window box can be determined by calculating the maximum auto-correlation value. Using these parameters, the digitized color photo can be automatically co-registered to AVIRIS image data where the average value of the pixels within the AVIRIS resolution is used to produce the co-registered brightness image. Furthermore, we also saved these parameters of each window box as an output file that can be used to co-register the classification image where the fractional snow-covered area image is produced as the ground truth.

We have collected more than 300 AVIRIS scenes with snow since 1994 over the different regions in North America. They covers a wide range of solar illumination, atmospheric, terrain, and snow conditions. Table 1 below summarizes the collected AVIRIS image data. We can access large amount of the ground truth data by using these digitized photo images of very high spatial resolution along with spectral information from AVIRIS image data.

Location	Sierra Nevada (U.S)	Cascades (U.S)	Rocky Mt. (U.S)	Boreas Forest (Canada)	Total
AVIRIS	198	68	89	12*	367

Table 1: The collected AVIRIS airborne image data. * Indicates that the color infrared photo is not available right now.

EXAMPLES OF ALGORITHM PERFORMANCE AND ITS VALIDATION

To demonstrate the algorithm performance and its validation, we show an example using the simulated ASTER 9 band visible-Infrared image data from AVIRIS scenes. Surface apparent reflectance images of AVIRIS were derived using the approach described by [21]. This approach rely on the atmospheric models of the MODTRAN3 radiative transfer code to generate a series of look-up table for an AVIRIS scene collected at a specific latitude and longitude on a specific date. The water vapor, surface pressure height, and aerosol optical depth were characterized to use in the surface spectral reflectance calculation. The ASTER's spectral response function for each band was convolved with AVIRIS data and re-sampled to 30-m resolution to generate the simulated ASTER visible-Infrared image data.

Figure 2 compares the snow covered maps derived from the simulated ASTER image data on left, with one derived from high-resolution , infrared color photos on right. The brightness is proportional to snow fraction at each

pixel. The black regions are snow-free. This example represents a case where snow cover is characterized as more of a continuum in spatial distribution. The major part of snow cover is fully covered by snow. The mixed pixels mainly occur at low elevation. At high elevation regions, the snow-mixed pixels are mainly distributed at high surface relief or large slope areas. In our algorithm of steps 1 and 2, some 783 snow-free endmembers were initially selected. By running step 3, 551 of these plus 69 bare surface and vegetation spectral endmembers were finally identified as the reference snow-free endmembers for the multi-endmember snow unmixing, in which 17 % and 8 % of these endmembers are identified from the spectral library data for bare surface and vegetation, respectively. The remaining ones are identified as local endmembers from the scene itself. From scene to scene, these values could vary greatly due to the limited available field spectral measurements. Identifying local spectral endmembers is essential for insuring the accuracy of snow fraction estimation. For snow, 872 endmembers were selected through steps 1 and 2; these cover a wide range snow and terrain conditions. There were 736 classes determined through steps 1 and 2 for the look-up table of the mixed pixels. It is 0.8 % of total mixed pixels. To compare the accuracy of the ASTER-derived snow map, we performed several tests. The first test was to check errors in mis-classification of level-0 classifiers. In this example, 3.8 % of the snow-free pixels were mis-classified as being snow mixed pixels. Some 1.3 % of the snow mixed pixels were mis-classified as being snow-free. The relative error for estimating total snow covered area, as the second test, is 1.7 %. The RMSE for snow mixed pixels is 8.4 %. In computation aspect, it took about 38 CPU hours to generate the snow map on a 500 MHz alpha workstation if we ran all of the mixed pixels by the multi-endmember unmixing. However, it only took 18 minutes by using look-up table approach.

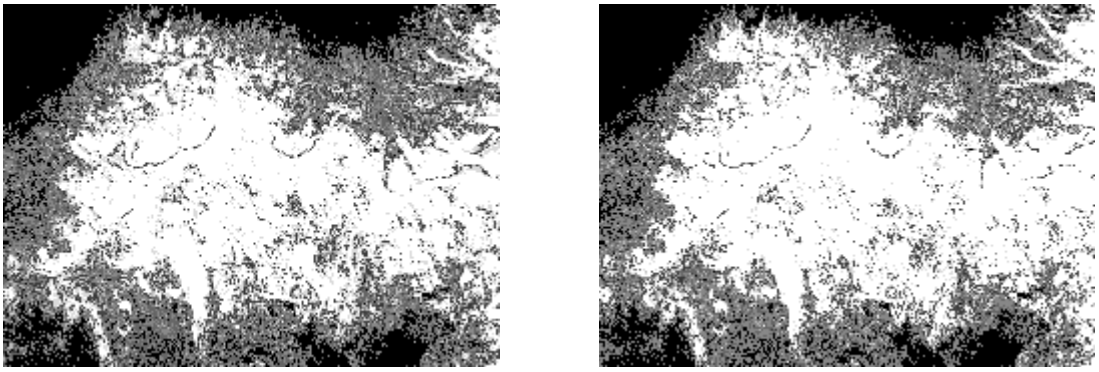

The cost is that the accuracy was reduced from 6.9 % to 8.4 % in snow fraction estimation.

Figure 2. The comparison of the snow covered maps derived from the simulated ASTER image data on left, with one derived from high-resolution , infrared color photos on right. The brightness is proportional to snow fraction at each pixel.

DISCUSSION

Accessing the ground truth of snow covered area is a key component for snow mapping algorithm development and validation. The commonly used techniques are either user-supplied or a low elevation aerial photo. The former has no means of validation. The later provides a high-resolution photo within a few meters. However it may be obtained at different times with the satellite or airborne data to be evaluated, which results in different solar illumination geometry. The ground truth for snow covered area might have changed significantly. Furthermore, only a small portion of the low elevation photo can be used to access the ground truth, even if the photo and satellite or airborne data were taken at nearly the same time. This is due to the elevation difference between these two instruments, which causes geometric distortion in a resolution and in sensor viewing geometry. The former results in a co-registering difficulty. The later results in that a low elevation photo that cannot represent what the satellite “sees”, especially in alpine and forest regions where terrain and trees may block the view of the camera. Therefore, only a small portion, -- that with a close-to-nadir view of the low elevation photo -- can be used for accessing ground truth. In contrast, the advantages of using color infrared photo on board ER-2 are: 1) no difference between the color infrared photo to be used to obtain the ground truth data and the image data (AVIRIS) to be used to simulate the satellite measurements since they are taken simultaneously, 2) similar solar illumination and sensor viewing geometry since the instruments are on the same platform, and 3) covers large area (AVIRIS

coverage). With high spectral measurements of AVIRIS, most of the visible infrared optical satellite measurements can be simulated with high accuracy even before launching of the satellite. Therefore, AVIRIS image data and the color near-infrared photo provide a unique tool for snow mapping algorithm development and validation.

The current techniques on estimation of snow fraction by linear unmixing mainly differ in the methods of selecting the reference spectral endmembers for the unmixing process. As we have demonstrated in this study, terrain has great impact on unmixing process. Each technique has its own advantages and dis-advantages. The approach presented in this study is based on compromising the advantages and disadvantages of each current technique. The tested results indicate the snow cover can be estimated by ASTER image data at sub-pixel resolution with high accuracy. It will provide the high accurate snow maps for predicting snow-melting runoff and hydrological applications.

REFERENCES

[1] J. Dozier and D. Marks, Snow mapping and classification from Landsat Thematic Mapper data, *Ann. Glaciol.*, vol.9, pp. 97-103, 1987.

[2] J. Dozier, Spectral signature of alpine snow cover from the Landsat Thematic Mapper, *Remote Sens. Environ.*, 28:9-22, 1989.

[3] S. E. Marshall and S. G. Warren, Parameterization of snow albedo for climate models, In *Large Scale Effects of Seasonal Snow Cover*, IAHS Publication 166, 43-50, 1987.

[4] R. F. Harrington, K. Elder, and R. C. Bales, Distributed snowmelt modeling using a clustering algorithm, *Biogeochemistry of Seasonally Snow-Covered Catchments*, IAHS Publication 228:167-174, 1995.

[5] J. Martinec and A. Rango, Areal distribution of snow equivalent evaluated by snow cover monitoring, Water Resources Research 17(5):1480-1488, 1981.

[6] G. Vane, R. O. Green, T. G. Chrien, and H. T. Enmark, The airborne visible and infrared imaging spectrometer, *Remote Sens. Environ.*, 44(2-3):127-143, 1993.

[7] G. Vane and A. F. H. Goetz, Terrestrial imaging spectrometry: Current status, future trends, *Remote Sens. Environ.*, 44(2-3):117-126, 1993.

[8] A. Rango, An international perspective on large-scale snow studies, Hydrological sciences bulletin, 50(4):225--238, 1985.

[9] J. Martinec and A. Rango, Interpretation and utilization of areal snow-cover data from satellites, *Ann. Glaciol.*, 9, 1987.

[10] T. R. Carroll, J. V. Baglio, J. P. Verdin, and E. W. Holroyd, Operational mapping of snow cover in the United States and Canada using airborne and satellite data, *Proceedings IGARSS '89*, IEEE No. 89CH2768-0, vol. 3, pp. 1257-1259, 1989.

[11] D. K. Hall, G. A. Riggs, and V. V. Salomonson, Development of methods for mapping global snow cover using Moderate Ersolution Imaging Spectroradiometer data, *Remote Sensing Environment*, 54:127-140, 1995.

[12] J. W. Boardman and A. F. H. Geotz, Sedimentary facies analysis using AVIRIS data: A geophysical inverse problem, In *Proceedings of the third annual JPL airborne workshop*, pp.4-13, Jet Propulsion Laboratory, JPL Publication 91-28, 1991.

[13] A. W. Nolin, J. Dozier, and L. A. K. Mertes, Mapping alpine snow using a spectral mixture modeling technique, *Ann. Glaciol.* 17:121-124, 1993.

[14] A. W. Nolin and J. Dozier, Estimating snow grain size using AVIRIS data, *Remote Sens. Environ.*, 44(2-3):231-238, 1993.

[15] T. H. Painter, D. A. Roberts, R. O. Green, and J. Dozier, The effect of grain size on spectral mixure analysis of snow-covered area from AVIRIS, *Remote Sens. Environ.*, 65-320-332, 1998.

[16] W. Rosenthal and J. Dozier, Automated mapping of montane snow cover at sub-pixel resolution from the Landsat Thematic Mapper, *Water Resour. Res.*, 32(1): 115-130, 1996.

[17] W. Rosenthal, Automated snow mapping at sub-pixel resolution from NOAA--AVHRR data; final report: programs for estimating sub-pixel snow-covered area, Technical report, U.S. Army Cold Regions Research and Engineering, Laboratory, Hanover, NH, 1996.

[18] D. A. Roberts, M. Gardner, R. Church, S. Ustin, G. Scheer, and R. O. Green, Mapping chaparral in the Santa Monica mountains using multiple endmember spectral mixture models, *Remote Sens. Environ*., 65:267-279, 1997.

[19] S. G. Warren and W. J. Wiscombe, A model for the spectral albedo of snow, II, Snow containing atmospheric aerosols, Journal of the Atmospheric Sciences, vol. 37, no. 12, pp. 2734--2745, 1980.

[20] W. J. Wiscombe and S. G. Warren, A model for the spectral albedo of snow, I, pure snow, Journal of the Atmospheric Sciences, vol. 37, no. 12, pp. 2712--2733, 1980.

[21] R. O Green, D. A. Roberts, and J. A James, Characterization of the atmosphere and inversion of AVIRIS calibrated radiance to apparent surface reflectance, in *Proceedings of The Sixth Annual JPL Airborne Earth Science Workshop*, vol., 1, 1996.